Plasmonic Photocatalysis

International Edition: DOI: 10.1002/anie.201606734
German Edition: DOI: 10.1002/ange.201606734

Gold-Nanoparticle-Loaded Carbonate-Modified Titanium(IV) Oxide Surface: Visible-Light-Driven Formation of Hydrogen Peroxide from Oxygen

*Miwako Teranishi, Riyoko Hoshino, Shin-ichi Naya, and Hiroaki Tada**

Abstract: *Gold nanoparticle-loaded rutile TiO_2 with a bimodal size distribution around 10.6 nm and 2.3 nm (BM-Au/TiO_2) was prepared by the deposition precipitation and chemical reduction (DP-CR) technique. Visible-light irradiation ($\lambda >$ 430 nm) of the BM-Au/TiO_2 plasmonic photocatalyst yields 35 μM H_2O_2 in aerated pure water at irradiation time (t_p) = 1 h, and the H_2O_2 concentration increases to 640 ± 60 μM by the addition of 4% HCOOH as a sacrificing electron donor. Further, a carbonate-modified surface BM-Au/TiO_2 (BM-Au/TiO_2-CO_3^{2-}) generates a millimolar level of H_2O_2 at t_p = 1 h with a quantum efficiency (Φ) of 5.4% at λ = 530 nm under the same conditions. The recycle experiments confirmed the stable performance of BM-Au/TiO_2.*

Hydrogen peroxide (H_2O_2) has attracted much interest as not only a "green" oxidant for organic synthesis[1] but also the source for a new fuel cell.[2] Presently, most H_2O_2 is produced by the anthraquinone oxidation process through the many steps needing large amounts of input energy and organic solvent.[3] As alternative, various chemical and physical methods have recently been studied.[4] If H_2O_2 can be produced from O_2 and water, a sustainable energy cycle is completed by combining with the H_2O_2-based fuel cell (Scheme 1). For this endergonic reaction to proceed, the effective use of sunlight with a broad energy peak locating from 500 nm to 650 nm is desirable as an energy source [Eq. (1)].

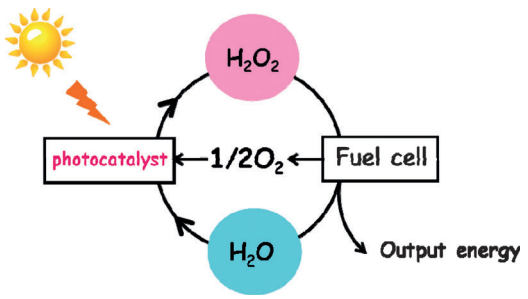

Scheme 1. Solar oxygen cycle using the H_2O_2-based fuel cell.

$$1/2\,O_2 + H_2O \rightarrow H_2O_2 \qquad \Delta_r G^0 = +116.8\,\mathrm{kJ\,mol^{-1}} \tag{1}$$

UV-light irradiation of TiO_2 in water yields H_2O_2, but the H_2O_2 concentration is only limited to micromolar levels.[5] We have reported that a millimolar level of H_2O_2 can be produced from O_2 by UV-light irradiation of gold nanoparticle (NP)-loaded TiO_2 (Au/TiO_2) in an aqueous solution of ethanol.[6] The photocatalytic synthesis of H_2O_2 has been intensively studied to increase its steady-state concentration by using heterogeneous photocatalysts such as Au-Ag/TiO_2,[7] graphene oxide-TiO_2,[8] and silicon nanowire-TiO_2-Au.[9] A coming challenge is to use the visible light as the energy source for the effective sunlight utilization. So far, several reports on the H_2O_2 synthesis from O_2 using visible-light photocatalysts including graphitic carbon nitride (g-C_3N_4)-based photocatalysts[10,11] have been published. Particularly, a high Φ value of about 10% has been achieved at λ = 420 nm in the g-C_3N_4 system; however, it is inactive at λ > 500 nm.[11] On the other hand, the plasmonic photocatalysts represented by Au/TiO_2 have appeared as a new class of photocatalysts.[12] By using the Au/TiO_2 plasmonic photocatalyst, various oxidative transformations including alcohol to carbonyl compounds,[13,14] thiol to disulfide,[15] benzene to phenol,[16] and amine to imine[17] have been developed. A bimodal (BM)-Au/TiO_2 plasmonic photocatalyst has been shown to have a potential for the application to the reductive transformation.[18] So far, the BM-Au/TiO_2 plasmonic photocatalyzed reaction is only limited to the reduction of nitrobenzene analogs to the corresponding azobenzenes.

Herein we report the visible-light-driven reduction of O_2 to H_2O_2 in pure water by the BM-Au/TiO_2 plasmonic photocatalyst, further showing that carbonate-surface modified BM-Au/TiO_2 (BM-Au/TiO_2-CO_3^{2-}) yields a millimolar level of H_2O_2 in the presence of formic acid (HCOOH). BM-Au/TiO_2 was prepared by the DP-CR technique.[18] The visible-light activity of Au/TiO_2 depends on the crystal form of TiO_2, and rutile is superior to anatase[14] in contrast to the UV-light activity of TiO_2 for most photocatalytic reactions.[19] At the first step, large Au NPs were loaded on rutile TiO_2 (L-Au/TiO_2) by the DP method.[20] At the second step, $[Au(OH)_3Cl]^-$ complex ions were adsorbed on the TiO_2 surface of L-Au/TiO_2, and then, they were reduced by $NaBH_4$ to yield small Au NPs. For comparison, the second CR procedure was applied to unmodified TiO_2 to produce small Au NP-loaded TiO_2 (S-Au/TiO_2). The Au 4f X-ray photoelectron spectra of Au/TiO_2 have two signals at 87.0 and 83.3 eV due to the

[*] M. Teranishi, Dr. S. Naya
Environmental Research Laboratory, Kindai University
3-4-1, Kowakae, Higashi-Osaka, Osaka 577-8502 (Japan)
R. Hoshino, Prof. Dr. H. Tada
Department of Applied Chemistry
School of Science and Engineering, Kindai University
3-4-1, Kowakae, Higashi-Osaka, Osaka 577-8502 (Japan)
E-mail: h-tada@apch.kindai.ac.jp

Supporting information for this article can be found under: http://dx.doi.org/10.1002/anie.201606734.

emissions from the Au 4f 5/2 and Au 4f 7/2 orbitals for metallic Au, respectively.[21] Evidently, the Au^{III} complex adsorbed on TiO_2 is reduced to metallic Au by $NaBH_4$ at the second step.

Transmission electron microscopy (TEM) images (see Figure S1 in the Supporting Information) and the Au particle size distribution for L-Au/TiO_2 show that Au particles with a mean size (d) of 9.7 nm (standard deviation $\sigma = 1.6$ nm) are highly dispersed on the TiO_2 surface. In BM-Au/TiO_2, L-and S-Au particles with d values of 10.6 nm ($\sigma = 4.0$ nm) and 2.3 nm ($\sigma = 1.3$ nm), respectively, are separately formed on TiO_2. For S-Au/TiO_2, the d value was 2.3 nm ($\sigma = 1.0$ nm). The Au loading amounts were determined to be 0.52 wt% for S-Au/TiO_2, 0.49 wt% for L-Au/TiO_2, and 0.88 wt% for BM-Au/TiO_2 by inductively coupled plasma spectroscopy.

Further, CO_3^{2-} ions were adsorbed on the BM-Au/TiO_2 surface from a 100 mM Na_2CO_3 aqueous solution (BM-Au/TiO_2-CO_3^{2-}). Figure 1 A shows diffuse reflectance Fourier transform infrared (DRIFT) spectra for BM-Au/TiO_2-CO_3^{2-}, and TiO_2 for comparison. In the spectrum of TiO_2, a signal assignable to the stretching vibration of the surface Ti-OH groups [ν(Ti_s-OH)] is observed at 3695 cm^{-1}, while in the 1200–1800 cm^{-1} region, a signal due to the deformation vibration of adsorbed water [δ(H_2O)] is situated at 1637 cm^{-1}. The spectrum of BM-Au/TiO_2-CO_3^{2-} has additional two characteristic signals at 1520 and 1448 cm^{-1}, which can be assigned to the antisymmetric [ν_a(OCO)] and symmetric [ν_s(OCO)] stretching vibrations for the CO_3^{2-} ions adsorbed on the TiO_2 surface with a bidentate structure.[22] Also, the ν(Ti_s-OH) signal significantly weakens with the adsorption of CO_3^{2-} ions. Evidently, CO_3^{2-} ions are adsorbed on the Ti_s-OH sites of BM-Au/TiO_2-CO_3^{2-} through chelation. Figure 1 B shows UV/Vis absorption spectra of TiO_2 and Au/TiO_2, and the solar spectrum. While rutile TiO_2 only has absorption at $\lambda < 410$ nm, the Au NP loading induces strong and broad absorption due to the localized surface plasmon resonance (LSPR) in the visible region. The LSPR peaks for S-Au/TiO_2 and L-Au/TiO_2 are located around 550 nm and 580 nm, respectively. The spectrum of BM-Au/TiO_2 is likely the sum of the absorptions of S-Au/TiO_2 and L-Au/TiO_2 with an apparent LSPR peak at 566 nm, well matching with the solar spectrum. The spectrum hardly changes with the CO_3^{2-} adsorption, which also supports the conclusion that CO_3^{2-} ions are selectively adsorbed on the TiO_2 surface of BM-Au/TiO_2-CO_3^{2-}. The larger Au loading amount is responsible for the stronger absorption intensity.

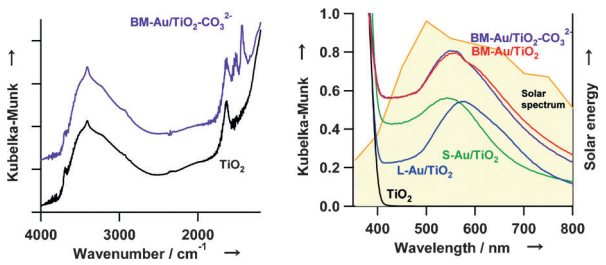

Figure 1. A) DRIFT spectra for CO_3^{2-} ion-adsorbed BM-Au/TiO_2, and TiO_2 for comparison. B) UV/Vis absorption spectra for the unmodified TiO_2 and Au/TiO_2 samples and the solar spectrum.

We examined the photocatalytic activity of BM-Au/TiO_2 for the O_2 reduction reaction (ORR) to H_2O_2 without and with sacrificing electron donors (4% C_2H_5OH or HCOOH), and that of BM-Au/TiO_2-CO_3^{2-} in the presence of 4% HCOOH. Catalyst was added in an aerated aqueous solution (10 mL), and H_2O_2 generated under irradiation of visible light ($\lambda > 430$ nm) at 298 K was quantified by the iodometric titration. To evaluate the activity at the comparable Au amount, 20 mg of S- and L-Au/TiO_2 was added in each run, while 10 mg of BM-Au/TiO_2 and BM-Au/TiO_2-CO_3^{2-} were used. Figure 2 A shows time courses for the H_2O_2 generation in the BM-Au/TiO_2 system. No H_2O_2 was generated in the dark. Visible-light irradiation of BM-Au/TiO_2 in pure water yields 35 ± 5 μM H_2O_2 at $t_p = 20$ minutes. Since the Au/TiO_2 plasmonic photocatalyst oxidizes water under visible-light irradiation,[23,24] the total reaction is expressed by Equation (1). The addition of the electron donors greatly enhances the reaction, and the H_2O_2 concentration increases with increasing t_p. In the HCOOH-added system, the H_2O_2 concentration reaches 640 ± 60 μM at $t_p = 1$ h. We have recently reported that a decreasing pH of the reaction solution accelerates the Au/TiO_2 photocatalytic ORR to H_2O_2 under UV-light irradiation.[25] The pH values of the C_2H_5OH- and HCOOH-added solutions were 7.2 and 1.7, respectively. Thus, HCOOH works as not only a good electron donor but also as a pH-regulating agent. Gas chromatography confirmed the formation of CO_2 during the reaction (Figure S2). The total reaction is exergonic, and written by Equation (2).

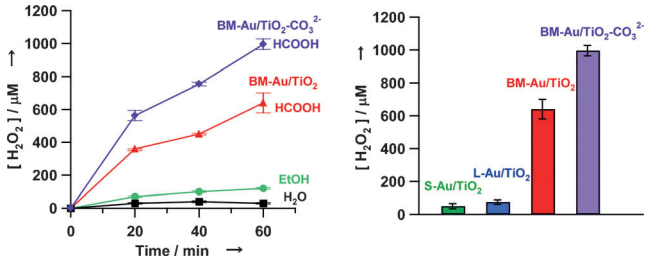

Figure 2. A) Time courses for the BM-Au/TiO_2-phatocatalytized H_2O_2 generation in the absence (black) and presence of 4% C_2H_5OH (green) and 4% HCOOH (red), and for the BM-Au/TiO_2-CO_3^{2-}-photocatalyzed H_2O_2 generation with 4% HCOOH (purple) under irradiation of visible light ($\lambda > 430$ nm, light intensity integrated from 420 to 485 nm = 4.0 mW cm^{-2}) at 298 K. B) Photocatalytic activity of S-Au/TiO_2, L-Au/TiO_2, BM-Au/TiO_2, and BM-Au/TiO_2-CO_3^{2-} for the reduction of O_2 to H_2O_2 in an aqueous solution containing 4% HCOOH (pH 1.7) in the dark and under irradiation of visible light ($\lambda > 430$ nm, light intensity integrated from 420 to 485 nm = 4.0 mW cm^{-2}) at 298 K.

$$O_2 + HCOOH \rightarrow H_2O_2 + CO_2 \qquad \Delta_r G^0 = -153.4\,kJ\,mol^{-1} \qquad (2)$$

Surprisingly, BM-Au/TiO_2-CO_3^{2-} exhibits much higher activity than BM-Au/TiO_2 under the same conditions, and the H_2O_2 concentration increases with an increase in t_p. Since the pH of the solution remained at 1.7, the possibility can be

excluded that the carbonate effect is due to a pH change.

The photocatalytic activities of the Au/TiO_2 samples were examined in the presence of 4% HCOOH. Figure 2B compares the concentration of H_2O_2 generated at $t_p = 1$ h. The H_2O_2 concentration in the BM-Au/TiO_2 system (640 ± 60 μM) far exceeds the sum of the H_2O_2 concentrations in S-Au/TiO_2 (50 μM) and L-Au/TiO_2 (75 μM). Further, in the BM-Au/TiO_2-CO_3^{2-} system, the H_2O_2 concentration reaches about 1 mM. Further, the reaction was performed in the BM-Au/TiO_2-CO_3^{2-} system using a green light emitting diode as a light source, and a quantum efficiency was calculated from the equation of $\Phi = 2 \times$ (molecule number of H_2O_2 formed)/(incident photon number) to be 5.4% at $\lambda = 530$ nm.

The life time as well as the activity is the key factor for the catalysts. To examine the stability of the BM-Au/TiO_2 photocatalyst, recycle experiments were carried out (Figure S3). When the catalyst was not washed after the reaction, the activity gradually decreased with an increase in the recycle number (N). Then, the catalyst was reused by washing with water after each run. Unexpectedly, the photocatalytic activity increases at $N = 2$ to be maintained at least $N \leq 5$. These intriguing results are discussed in more detail later in connection with the action mechanism of the present plasmonic photocatalyst.

Mesoporous TiO_2 nanocrystalline films were formed on fluorine-doped tin oxide electrodes (TiO_2/FTO) by the doctor blade method (see the Supporting Information), and CO_3^{2-} ions were chemisorbed on the surface (CO_3^{2-}-TiO_2/FTO). To gain information about the surface modification effect by CO_3^{2-} ions, electrochemical (EC) measurements were carried out for a three-electrode EC cell containing the TiO_2/FTO structure with and without carbonate surface modification (working electrode) | Ag/AgCl (reference electrode) | aerated 0.1M $NaClO_4$ aqueous solution with and without 1 mM H_2O_2 | glassy carbon (counter electrode). Figure 3A shows linear sweep voltammograms for the TiO_2/FTO and CO_3^{2-}-TiO_2/FTO electrodes in the absence and presence of O_2 and H_2O_2. In the unmodified TiO_2/FTO electrode system, the current onset potential (E_{on}) is located at −0.1 V without O_2 and H_2O_2, at 0 V with O_2 and without H_2O_2, and at +0.2 V without O_2 and H_2O_2. The E_{on} with O_2 and H_2O_2 remains +0.2 V. These results indicate that the reductions start for H_2O_2 at +0.2 V [$E_{on}(H_2O_2)$], for O_2 at +0 V [$E_{on}(O_2)$], and for TiO_2 at −0.1 V [$E_{on}(TiO_2)$]. In the CO_3^{2-}-TiO_2/FTO electrode system, the current with O_2 and H_2O_2 significantly decreases, and the E_{on} is almost in agreement with the $E_{on}(O_2)$. Also, the value with O_2 and without H_2O_2 is rather close to the $E_{on}(TiO_2)$. Clearly, the surface modification with CO_3^{2-} ions effectively suppresses the reductions of H_2O_2 by the TiO_2/FTO electrode.

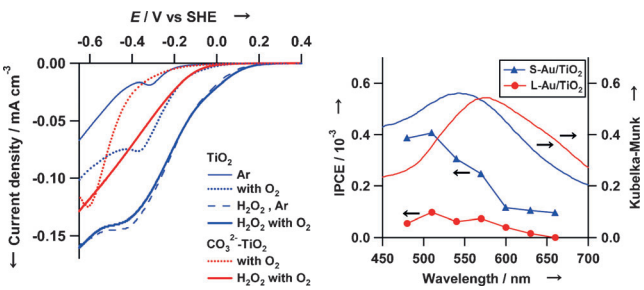

Figure 3. A) Dark current–potential (E/V vs. standard hydrogen electrode, SHE) curves for TiO_2/FTO electrodes without and with the carbonate surface modification in 0.1 M $NaClO_4$ aqueous solution in the absence and presence of O_2 and 1 mM H_2O_2 (pH ≈ 6.2). B) IPCE action spectra for the three-electrode PEC cells with a structure of S-Au/TiO_2/FTO and L-Au/TiO_2/FTO (photoanode) | Ag/AgCl (reference electrode) | 0.1 M $NaClO_4$ electrolyte solution containing 4% formic acid | glassy carbon (cathode), and the absorption spectra for the photoanodes for comparison.

Further to clarify which of S- and L-Au NPs acts as the oxidation site in BM-Au/TiO_2, we carried out photoelectrochemical (PEC) measurements by using S- and L-Au/TiO_2 nanocrystalline films formed on FTO (Au/TiO_2/FTO) as the photoanode (see the Supporting Information). A three-electrode PEC cell with the structure of photoanode | Ag/AgCl (reference electrode) | 0.1M $NaClO_4$ electrolyte solution containing 4% HCOOH | glassy carbon (cathode) was fabricated. In the photocurrent time curves for the S- and L-Au/TiO_2/FTO photoanode cells at the rest potential in the dark, irradiation of visible light ($\lambda > 430$ nm) causes anodic photocurrent in each system (Figure S4). A much larger photocurrent is observed for the S-Au/TiO_2/FTO system than the L-Au/TiO_2/FTO system. As suggested by the results on the particulate system, HCOOH should be oxidized on the surface of Au NPs of the Au/TiO_2/FTO photoanode, while O_2 is reduced at the cathode in this PEC cell. The action spectrum is also important for elucidating the reaction mechanism. The action spectra of the incident photon-to-current efficiency (IPCE) for the Au/TiO_2/FTO photoanode cells were measured using optical filters with varying cut-off wavelength.[26] Figure 3B shows the action spectra of IPCE for the present PEC cells, and the absorption spectra of the photoanodes for comparison. The IPCE value for the S-Au/TiO_2/FTO system is significantly larger than that for the L-Au/TiO_2/FTO system in the 475–660 nm range. The IPCE in each system increases with decreasing wavelength of incident light with only a weak shoulder near the LSPR peak, whereas a peak is observed near the LSPR-peak wavelength in the action spectra for several Au/MO-plasmonic photocatalytic reactions.[14,15,17,27] A similar action spectrum has recently been reported for the water oxidation by a PEC cell employing Au/$SrTiO_3$ as the photoanode.[28] The absorption intensity of the interband transition monotonically increases with decreasing wavelength, and thus, the reaction may be triggered by the excitation of the 5d-6sp transition of Au NP in addition to its LSPR. These results are consistent with the previous conclusion that the excited electrons are transferred from S-Au NPs to L-Au NPs by way of TiO_2.[18] As a result of the decrease in d from 10.6 to 2.3 nm, the density of states (DOS) of Au NPs greatly lowers.[29] While in the small Au NPs, the small DOS increases the entropic driving force for the forward electron transfer from Au NP to TiO_2 with that for the back electron transfer simultaneously decreased, the opposite situation is valid for L-Au NPs.[30] The difference in the entropic driving force for the electron transfer at the S-Au NP/TiO_2 and the L-Au NP/TiO_2 interfaces rationalizes the electron transport from S-Au NPs to L-Au NPs through TiO_2 in BM-Au/TiO_2.

On the basis of these results above, the mechanism of the BM-Au/TiO_2 plasmonic photocatalyzed-reduction of O_2 to H_2O_2 is proposed (Scheme 2). Visible-light irradiation of BM-Au/TiO_2 gives rise to the interfacial electron transfer from small-to-large Au NP through the conduction band (CB) of

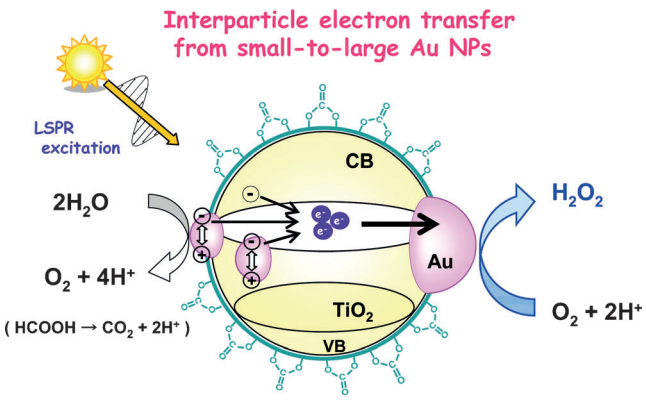

Scheme 2. A mechanism proposed for the BM-Au/TiO_2-CO_3^{2-}plasmonic photocatalyzed-reduction of O_2 to H_2O_2.

TiO_2.[18] The Fermi energy (E_F) of S-Au NPs lowers, while the E_F of L-Au NPs rises up. As a result, the oxidizing and reducing abilities are induced on S- and L-Au NPs, respectively. In pure water, H_2O is oxidized to O_2 and H^+ on the S-Au NP surface of Au/TiO_2, of which visible-light activity steeply increases at the Au mean particle size < 4 nm.[30] In the presence of HCOOH, it is preferentially oxidized to CO_2 and H^+ on the S-Au NP surface. On the other hand, the ORR proceeds on the L-Au NP surface. Thermodynamically, the potential of the electrons in the CB of rutile TiO_2 (flat-band potential, $E_{fb} = +0.04$ V at pH 1.0 vs. SHE)[31] is insufficient for the one-electron ORR ($E^0(O_2/HO_2) = -0.046$ V vs. SHE)[32] to proceed, but is sufficient for the two-electron ORR ($E^0(O_2/H_2O_2) = +0.695$ V vs. SHE).[32] In this system, due to the electron pool effect[33] and electrocatalysis for the two-electron ORR of the L-Au NP,[34] O_2 would be effectively reduced to H_2O_2 on the surface. Similar effects have been suggested for the Cu^{II} ions in a visible-light-responsive Cu^{II}-grafted rutile TiO_2 system.[35] Eventually, in the BM-Au/TiO_2 system, S-Au NPs highly dispersed on TiO_2 work as an antenna for the incident light to inject electrons into TiO_2, and the collected electrons in L-Au NPs are effectively used for the two-electron ORR because the Au/TiO_2-catalyzed H_2O_2 decomposition is significantly suppressed at $d < 3$ nm and $d >$ 8 nm.[6] The much higher photocatalytic activity of BM-Au/TiO_2 than S- Au/TiO_2 and L-Au/TiO_2 can be mainly attributed to the long-range charge separation by the visible-light-induced vectorial interfacial electron transfer (S-Au→CB-(TiO_2)→L-Au). However, H_2O_2 once produced undergoes degradation via the reduction of the surface peroxide species (Ti_s-OOH), resulting from the reaction of H_2O_2 with the surface Ti-OH (Ti_s-OH) groups, by the CB-electrons in TiO_2.[36] CO_3^{2-} ions chemisorbed on TiO_2 suppress the Ti_s-OH-mediated reductive degradation pathway. Consequently, the extremely high visible-light activity of BM-Au/TiO_2-CO_3^{2-} would stem from the compatibility of the effective charge separation in the BM-Au/TiO_2 heterostructure and the suppression of the TiO_2 surface-mediated H_2O_2 decomposition by the surface modification with CO_3^{2-} ions. The reaction in the presence of HCOOH yields CO_2 [Eq. (2)], which could partly be adsorbed on the TiO_2 surface during the reaction. These considerations explain the increase in the activity at $N \geq 2$ (Figure S3). The surface-fluorination of TiO_2 was previously reported to be effective in increasing the H_2O_2 concentration under irradiation of UV light.[37,38]

In summary, this study has shown that irradiation of visible light ($\lambda > 430$ nm) of BM-Au/TiO_2 in aerated pure water yields 35 μM H_2O_2, and the generation of a millimolar level of H_2O_2 with a Φ value of 5.4 % at $\lambda = 530$ nm has been achieved in the BM-Au/TiO_2-CO_3^{2-}system with HCOOH as an electron donor. We anticipate that this study presents the useful information about the design of the photocatalyst for the solar H_2O_2 synthesis.

Acknowledgements

This work was partially supported by a Grant-in-Aid for Scientific Research (C) (grant number 15K05654) and MEXT-Supported Program for the Strategic Research Foundation at Private Universities.

Keywords: hydrogen peroxide · oxygen reduction reaction · plasmonics · photocatalysis · solar chemical transformations

[1] K. Sato, M. Aoki, R. Noyori, *Science* **1998**, *281*, 1646–1647.
[2] Y. Yamada, S. Yoshida, T. Honda, S. Fukuzumi, *Energy Environ. Sci.* **2011**, *4*, 2822–2825.
[3] H. Reidl, G. Pfleiderer, Hydrogen peroxide. US Pat. 2215883, **1940**.
[4] J. M. Campos-Martin, G. Blanco-Brieva, J. L. G. Fierro, *Angew. Chem. Int. Ed.* **2006**, *45*, 6962–6984; *Angew. Chem.* **2006**, *118*, 7116–7139.
[5] R. Cai, Y. Kubota, A. Fujishima, *J. Catal.* **2003**, *219*, 214–218.
[6] M. Teranishi, S. Naya, H. Tada, *J. Am. Chem. Soc.* **2010**, *132*, 7850–7851.
[7] D. Tsukamoto, A. Shiro, Y. Shiraishi, Y. Sugano, S. Ichikawa, S. Tanaka, T. Hirai, *ACS Catal.* **2012**, *2*, 599–603.
[8] G.-H. Moon, W. Kim, A. D. Bokare, N.-E. Sung, W. Choi, *Energy Environ. Sci.* **2014**, *7*, 4023–4028.
[9] N. Kaynan, B. A. Berke, O. Hazut, R. Yerushalmi, *J. Mater. Chem. A* **2014**, *2*, 13822–13826.
[10] Y. Shiraishi, S. Kanazawa, Y. Kofuji, H. Sakamoto, S. Ichikawa, S. Tanaka, T. Hirai, *Angew. Chem. Int. Ed.* **2014**, *53*, 13454–13459; *Angew. Chem.* **2014**, *126*, 13672–13677.
[11] Y. Shiraishi, S. Kanazawa, Y. Sugano, D. Tsukamoto, H. Sakamoto, S. Ichikawa, T. Hirai, *ACS Catal.* **2014**, *4*, 774–780.
[12] C. Wang, D. Astruc, *Chem. Soc. Rev.* **2014**, *43*, 7188–7216.
[13] E. Kowalska, R. Abe, B. Ohtani, *Chem. Commun.* **2009**, 241–243.
[14] K. Kimura, S. Naya, Y. Jin-nouchi, H. Tada, *J. Phys. Chem. C* **2012**, *116*, 7111–7117.
[15] S. Naya, M. Teranishi, T. Isobe, H. Tada, *Chem. Commun.* **2010**, *46*, 815–817.

[16] Y. Ide, M. Matsuoka, M. Ogawa, *J. Am. Chem. Soc.* **2010**, *132*, 16762 – 16764.
[17] S. Naya, K. Kimura, H, Tada, *ACS Catal.* **2013**, *3*, 10 – 13.
[18] S. Naya, T. Niwa, T. Kume, H. Tada, *Angew. Chem. Int. Ed.* **2014**, *53*, 7305 – 7309; *Angew. Chem.* **2014**, *126*, 7433 – 7437.
[19] A. Y. Ahmed, T. A. Kandiel, T. Oekermann, D. Bahnemann, *J. Phys. Chem. Lett.* **2011**, *2*, 2461 – 2465.
[20] S. Tsubota, M. Haruta, T. Kobayashi, A. Ueda, Y. Nakahara, *Preparation of Catalysis V*, Elsevier, Amsterdam, **1991**.
[21] M. Someno, I. Yasumori, H. Bunseki, *Surface Analysis*, Kodansha, Tokyo, **1976**, p. 328.
[22] W. Su, J. Zhang, Z. Feng, T. Chen, P. Ying, C. Li, *J. Phys. Chem. C* **2008**, *112*, 7710 – 7716.
[23] Z. Liu, W. Hou, P. Pavaskar, M. Aykol, S. B. Cronin, *Nano Lett.* **2011**, *11*, 1111 – 1116.
[24] E. Thimsen, F. L. Formal, M. Grätzel, S. C. Warren, *Nano Lett.* **2011**, *11*, 35 – 43.
[25] M. Teranishi, S. Naya, H. Tada, *J. Phys. Chem. C* **2016**, *120*, 1083 – 1088.
[26] S. Naya, A. Inoue, H. Tada, *ChemPhysChem* **2011**, *12*, 2719 – 2723.
[27] Y. Tian, T. Tatsuma, *J. Am. Chem. Soc.* **2005**, *127*, 7632 – 7637.
[28] L. Liu, P. Li, B. Adisak, S. Ouyang, N. Umezawa, J. Ye, R. Kodiyath, T. Tanabe, G. V. Ramesh, S. Ueda, H. Abe, *J. Mater. Chem. A* **2014**, *2*, 9875 – 9882.
[29] R. W. Murray, *Chem. Rev.* **2008**, *108*, 2688 – 2720.
[30] M. Teranishi, M. Wada, S. Naya, H. Tada, *ChemPhysChem* http://dx.doi.org/10.1002/cphc.201600269.
[31] G. Cooper, J. A. Turner, A. J. Nozik, *J. Electrochem. Soc.* **1982**, *129*, 1973 – 1977.
[32] *Denki Kagaku Binran*, 5th ed., Electrochem. Soc. Jpn., Maruzen, Tokyo, **2000**.
[33] H. Tada, T. Kiyonaga, S. Naya, *Chem. Soc. Rev.* **2009**, *38*, 1849 – 1858.
[34] C. M. Sánchez-Sánchez, A. J. Bard, *Anal. Chem.* **2009**, *81*, 8094 – 8100.
[35] H. Irie, K. Kamiya, T. Shibanuma, S. Miura, D. A. Tryk, T. Yokoyama, K. Hashimoto, *J. Phys. Chem. C* **2009**, *113*, 10761 – 10766.
[36] X. Li, C. Chen, J. Zhao, *Langmuir* **2001**, *17*, 4118 – 4122.
[37] C. Minero, G. Mariella, V. Maurino, E. Pelizzetti, *Langmuir* **2000**, *16*, 2632 – 2641.
[38] H. Park, W. Choi, *J. Phys. Chem. B* **2004**, *108*, 4086 – 4093.

Received: July 11, 2016
Revised: August 2, 2016
Published online: ■■ ■■, ■■■■

Communications

Plasmonic Photocatalysis

M. Teranishi, R. Hoshino, S. Naya, H. Tada* ——— ▮▮▮▮–▮▮▮▮

Gold-Nanoparticle-Loaded Carbonate-Modified Titanium(IV) Oxide Surface: Visible-Light-Driven Formation of Hydrogen Peroxide from Oxygen

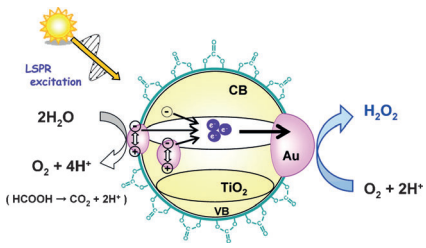

Solar hydrogen peroxide formation: Hydrogen peroxide was produced from molecular oxygen at millimolar level over bimodal gold-nanoparticle-decorated rutile by visible-light irradiation (see picture). Formic acid was used as electron donor and carbonate molecules were absorbed onto the rutile surface to minimize the simultaneous loss of hydrogen peroxide (LSPR = localized surface plasmon resonance).

